Nonlocal microscopic theory of Casimir forces at finite temperature

V. Despoja,[1,2,3,*] M. Šunjić,[1,2,†] and L. Marušić[4,‡]

[1]*Donostia International Physics Center (DIPC), P. Manuel de Lardizabal, ES-20018 San Sebastian, Basque Country, Spain*

[2]*Department of Physics, University of Zagreb, Bijenička 32, HR-10000 Zagreb, Croatia*

[3]*Depto. de Fýsica de Materiales and Centro Mixto CSIC-UPV/EHU, Facultad de Ciencias Quimicas, Universidad del Paýs Vasco, Apdo. 1072, E-20018 San Sebastian, Spain*

[4]*Maritime Department, University of Zadar, M. Pavlinovića b.b., HR-23000 Zadar, Croatia*

(Received 16 April 2010; revised manuscript received 19 January 2011; published 14 April 2011)

The interaction energy between two metallic slabs in the retarded limit at finite temperature is expressed in terms of surface polariton propagators for separate slabs, avoiding the usual matching procedure, with both diamagnetic and paramagnetic excitations included correctly. This enables appropriate treatment of arbitrary electron density profiles and fully nonlocal electronic response, including both collective and single-particle excitations. The results are verified by performing the nonretarded and long-wavelength (local) limits and showing that they reduce to the previously obtained expressions. Possibilities for practical use of the theory are explored by applying it to calculation of various contributions to the Casimir energy between two silver slabs.

DOI: 10.1103/PhysRevB.83.165421 PACS number(s): 13.40.−f, 71.36.+c, 03.70.+k

I. INTRODUCTION

Ever since Casimir postulated[1] the existence of attractive forces between neutral bodies due to the interaction of their ground-state (and later thermal) fluctuations, these effects fascinated the physics community and led to intense studies of their various aspects.[2–5] These became especially relevant with the advances in experimental techniques and their precision, applied to different geometries[5–9] and including finite temperatures. Several recent reviews[10–12] cover different theoretical and experimental aspects of this field.

As the ground-state energy shift arising from the virtual fluctuations of electromagnetic (EM) fields, the Casimir effect is an essentially quantum mechanical phenomenon. However, these fluctuations, in spite of their microscopic origin, in the long-wavelength limit correspond to the classical EM field excitations, i.e., bulk and surface polaritons, so that much of the theory can be, and was, done using classical electrodynamics based on the local description of the electron response in terms of the local dielectric function.[13,14] In such a local approach, the dispersion (i.e., wave-vector dependence) of this response mechanism was neglected. The local description proved extremely successful in many situations due to the fact that, at large separations between the objects, only the long-wavelength fields are relevant. However, improving this description, i.e., the treatment of electronic fluctuations (e.g., in metallic slabs, spheres, etc.), immediately leads to difficulties due to the intrinsic nonlocality of the electronic response in finite media resulting from the lack of translational invariance. This is the reason why most attempts, more or less successful, were based on semiempirical phenomenological corrections to the local theory based on the local dielectric function. The justification of such an approach, apart from simplicity, was based on the fact that, at large separations, long-wavelength fluctuations dominate and, indeed, nonlocal effects give negligible contributions to the Casimir energy.

Recently, a number of authors investigated the contribution of the EM modes to the Casimir force,[15–19] and even the effects of finite temperature and dissipation became a topic of discussion.[20–23] The common conclusion is that, no matter which level of approximation is used [hydrodynamic model,[15] empirical nonlocal susceptibility,[16] or self-consistent jellium model (limited to the linear Q correction to local Fresnel coefficients)],[17–19] nonlocal corrections are almost negligible at distances that are experimentally available (0.1 μm), i.e., around 1%, which is below the current experimental accuracy.

Previous calculations of the Casimir force obtained by using the random-phase approximation (RPA) dielectric tensor[3,4,21] show that the nonlocal effects give similar corrections to perfect metal Casimir force as the use of Drude (with dissipation) or experimental (wave-vector-independent) dielectric functions. They also show that the Casimir force calculated by using the RPA dielectric tensor with dissipation gives small additional corrections.[4,21] Therefore, it seems that, for semi-infinite metals, temperature effects and inclusion of dissipation modify Casimir interaction in the same manner as the nonlocal effects.[24] The principal role of nonlocal effects at room temperature for poor conductors has also been stressed in Ref. 25.

An interesting attempt to include nonlocal corrections[15–19] was made using the d-parameter approximations[26–28] based on the long-wavelength calculation of the shift in the position of the centroid of the induced charge density at the surface. The resulting change in the Casimir force, valid at large distances, can be interpreted as a shift of the effective surface position, which is very sensitive to the theoretical description of the electronic response. It would be interesting to compare these approximate results, which use the calculated d parameters,[29] with our exact results. However, this approach only concerns the p-polarized contributions, while the s-polarized reflectivity is unchanged in this theory.

In Sec. II, we first develop a formulation of the Casimir energy as the ground-state-energy (or free-energy) shift due to the electromagnetic coupling of the fluctuations in the two separate objects and, in Sec. III, we apply it to the retarded interaction between two metallic slabs. To take into account the nonlocal character of the fluctuations in a finite system, we avoid the standard approach[2] based on the matching procedure at the surfaces. Instead, we calculate the sum of all Feynman

diagrams for the ground-state fluctuations and show that the results for the Casimir free energy can be derived in a form similar to the usual one, but with the generalized reflectivities instead of the ones derived by the matching of EM fields.

Feynman diagrams for the coupled fluctuations can be separated into intraslab terms, which are responsible for electromagnetic interaction inside separated slabs, and interslab terms, describing the electromagnetic coupling between the slabs. We do not deal explicitly with the intraslab interactions since they are included in the surface polariton propagators.[30] We also show that s(TE) and p(TM) contributions to the Casimir energy can be separated, which enables us to study them quantitatively.

The resulting expressions for the Casimir free energy are given in terms of generalized reflectivities R_s and R_p, which are proportional to surface polariton propagators $D^{\rm ind}_{xx}$ and $D^{\rm ind}_{yy}$, respectively. This approach follows closely our theory of noncontact van der Waals interaction,[31] where a similar method was used to derive the expressions that include (in principle) exact wave-vector-dependent response functions in each metallic film. Here, we extend this method to treat the retarded interaction so that response functions and polariton propagators become matrices, but these can also be taken from Ref. 30.

In Sec. IV A, we show that these generalized expressions for the Casimir energy between two planar (metallic) slabs in the nonretarded limit correctly reduce to the usual van der Waals energy.[31] We can also relate them to the standard Lifshitz results in the long-wavelength limit obtained by neglecting dispersion and using the local dielectric function to describe the media, both for zero and finite temperatures.

In Sec. IV E, we apply our formalism to study Casimir energy between two silver slabs in the jellium model. Densities and electronic (current-current) response functions are calculated in the RPA using local-density approximation (LDA) self-consistent wave functions. This description includes both surface and bulk polaritons and their dispersion and (Landau) damping due to the excitation of electron-hole pairs, so there is no need for additional assumptions.

The expression for Casimir interaction includes both diamagnetic and paramagnetic contributions,[30] which enable us to separate and investigate, with a high level of accuracy, two kinds of corrections to the local Casimir energy. The diamagnetic term is sensitive to the details of the charge-density profile at the surface and the paramagnetic term arises from the intraband and interband electronic transitions, and contains essential nonlocal corrections.

We also checked (motivated, e.g., by Ref. 4) how our RPA nonlocal dielectric tensor (for a smooth density profile) and the local Drude dielectric function (for rectangular density profile) influence the s-mode reflectivity coefficient calculated in the Drude model without dissipation. Both models give qualitatively the same behavior for frequencies close to zero, where s reflectivity drops to zero very fast. This means that phenomenologically included dissipation mechanisms modify the Casimir force in a very similar way as the electron-hole excitations in our nonlocal theory. This is because the Casimir force is an integrated quantity and includes all possible fluctuations, so the contributions, e.g., from the low-energy tail of the damped Drude plasmon and from the continuum of electron-hole pairs, are difficult to distinguish.

The main contribution of this paper is that it provides a method for the microscopic calculation of generalized surface reflectivities, based on the self-consistently calculated electronic wave functions, from which we obtain nonlocal response functions and also smooth, charge-density profiles at surfaces without resorting to any matching procedure or Fresnel formulas. Although the results for Casimir energies might not differ significantly from those already obtained by standard methods, our formalism might become essential in the case of very thin metallic films at short distances.

II. FORMULATION OF THE PROBLEM

A. Ground-state energy of an interacting system

Following the procedure developed in Ref. 13, we shall briefly present how the ground-state-energy shift due to various interactions in the system can be expressed in terms of $\mathcal{S}$-matrix expansion. It is convenient to start from the finite-temperature formalism. Free-energy shift in the canonical ensemble when interaction is turned on can be written as

$$F - F_0 = -k_{\rm B}T \ln \langle \mathcal{S} \rangle, \tag{1}$$

where $k_{\rm B}$ is the Boltzman constant, T is the temperature of the system, and the thermodynamic average is taken with respect to the unperturbed (free) canonical distribution

$$\langle A \rangle = e^{F_0/k_{\rm B}T}\ {\rm Tr}\, e^{-H_0/k_{\rm B}T} A.$$

Here, F_0 and H_0 are unperturbed parts of the free energy and Hamiltonian, respectively. The average in (1) can also be written as

$$\langle \mathcal{S} \rangle = e^{\langle \mathcal{S} \rangle_{\rm con} - 1}, \tag{2}$$

where

$$\langle \mathcal{S} \rangle_{\rm con} = \sum_{n=1} \frac{(-1)^n}{n!} S_n^{\rm con}$$

and $S_n^{\rm con}$ is the sum of all closed connected diagrams that can be obtained in the nth order of the perturbation expansion. Furthermore, for every connected diagram in the nth order, there are $(n-1)!$ topologically equivalent diagrams, so we can write

$$S_n^{\rm con} = (n-1)!\ S_n^{\rm dif\ con},$$

where $S_n^{\rm dif\ con}$ are all topologically inequivalent diagrams of order n. The free-energy shift (1) now becomes

$$F - F_0 = -k_{\rm B}T \left\{ \sum_n \frac{(-1)^n}{n} S_n^{\rm dif\ con} - 1 \right\}. \tag{3}$$

In order to proceed, we shall anticipate some arguments given in more detail in Sec. II B. Our system consists of electromagnetic fields and electrons, and we shall consider the free-energy or ground-state-energy shift due to their interaction. In this case, $S_n^{\rm dif\ con}$ can be formally written (in the frequency space, omitting spatial coordinates) as

$$S_n^{\rm dif\ con} = \sum_k {\rm Tr}\{\Theta_n(i\omega_k) D(i\omega_k)\}, \tag{4}$$

which is shown in Fig. 1.

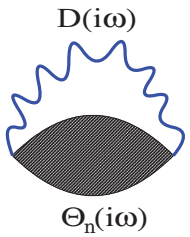

FIG. 1. (Color online) Feynman's diagram for $S_k^{\text{dif con}}$, i.e., the nth term in the perturbation expansion.

The summation in (4) is over discrete boson frequencies $\omega_k = 2k\pi k_B T$, where $k = 0,1,2,3,\ldots$, $\Theta_n(i\omega_k)$ is the polarization propagator of the system in the nth order, and $D(i\omega_k)$ is the electromagnetic field boson propagator. The trace operation is with respect to space coordinates and polarization. In Sec. II B, we present the detailed form of these propagators. Now we are able to use a very powerful relation that connects the temperature boson Green's functions with the retarded boson Green's functions:[13]

$$D(i\omega_k) = D^{\text{ret}}(i|\omega_k|), \quad \Theta(i\omega_k) = \Theta^{\text{ret}}(i|\omega_k|).$$

This relation is very useful because propagators that describe classical fields, e.g., currents or electromagnetic fields, are retarded boson Green's functions. Also, since for bosons $n = 2m$, and in this case all the frequencies are positive, expression (3) becomes

$$F - F_0 = -k_B T \left[\sum_{m=1} \frac{1}{2m} {\sum_{k=0}}' \text{Tr}\left\{ \Theta_{2m}^{\text{ret}}(i\omega_k) D^{\text{ret}}(i\omega_k) \right\} - 1 \right]. \tag{5}$$

The prime on the summation denotes that the $k = 0$ term is multiplied by a factor $\frac{1}{2}$.

B. Electromagnetic interaction between two objects

Now we shall apply expression (5) to calculate the interaction energy between two objects with nonoverlapping electron densities. We can start from the Hamiltonian

$$H = H_0 + V,$$

where H_0 is the energy of electrons in some local potential, and the interaction part V in the $\phi = 0$ gauge can be written as

$$V = -\frac{1}{c} \int d\mathbf{r}\, \mathbf{J}(\mathbf{r})\mathbf{A}(\mathbf{r}), \tag{6}$$

where the current operator is

$$\mathbf{J} = \mathbf{J}_1 + \mathbf{J}_2$$

with indices 1 and 2 denoting the two slabs and

$$\mathbf{J}_i = \frac{e\hbar}{2im} \left\{ \psi_i^+(\mathbf{r}) \nabla \psi_i(\mathbf{r}) - [\nabla \psi_i^+(\mathbf{r})] \psi_i(\mathbf{r}) \times -\frac{ie}{\hbar c} \psi_i^+(\mathbf{r}) \psi_i(\mathbf{r}) \mathbf{A}(\mathbf{r}) \right\}, \quad i = 1,2.$$

Here, ψ_i are electron field operators in the ith object, and $\mathbf{A}$ is the electromagnetic field operator. This interaction Hamiltonian treats the system consisting of two objects as unique, including (short-range) interaction inside individual objects and (long-range) interaction between different objects. Since we are interested only in the interaction between objects, we shall divide the vector potentials into the part mediating only between current fluctuations within the same object ($\mathbf{A}^S$), and the part mediating only between current fluctuations in different objects ($\mathbf{A}^L$). Now, the interaction Hamiltonian (6) can be written as

$$V = V_S + V_L. \tag{7}$$

Here, V_S and V_L have the same form as (6), with $\mathbf{A}$ replaced by $\mathbf{A}^S$ and $\mathbf{A}^L$, respectively. In order to separate the interobject energy shift from the intraobject one, interaction V_S can be included in H_0 and V_L treated as the perturbation

$$H = H_0^S + V_L,$$

where the Hamiltonian describing separate objects is

$$H_0^S = H_0 + V_S. \tag{8}$$

Note that this omission of the short-range interactions from the perturbation leads to the omission of the $k_B T$ term in (5).[13]

Some fluctuation diagrams of the fourth and eighth order with respect to V_L are shown in Fig. 2. Interaction between current fluctuations is mediated by the interobject photon propagator $\mathbf{D}^L$. Current fluctuations in the objects 1 and 2 are described by the current-current response functions $\mathbf{\Pi}_1$ and $\mathbf{\Pi}_2$, respectively. The $\mathbf{\Pi}_i$'s are not free response functions. They, in principle, contain all interaction terms arising from interaction V_S mediated by the intraobject photon propagator $\mathbf{D}^S$. For illustration, some terms in the expansion of $\mathbf{\Pi}_i$ are shown in Fig. 3(a). Local corrections to RPA diagrams shown in Fig. 3(b) are also mediated by $\mathbf{D}^S$. Furthermore, when an interobject photon is created in one of the objects, it can only be annihilated in the other object and nothing else can occur in between. Therefore, the propagator $\mathbf{D}^L$ is, in fact, the free photon propagator

$$\mathbf{D}^L = \mathbf{D}^0.$$

In the following, we shall neglect two-photon interobject exchange processes [Fig. 3(c)] in analogy with our theory of noncontact van der Waals forces.[31]

From Fig. 2, it can be recognized that the lowest order in the expansion of $\mathbf{\Theta}_m$ [which appears in Eq. (5)] is $\mathbf{\Theta}_2 = \mathbf{\Pi}_1 \mathbf{D}^0 \mathbf{\Pi}_2$,

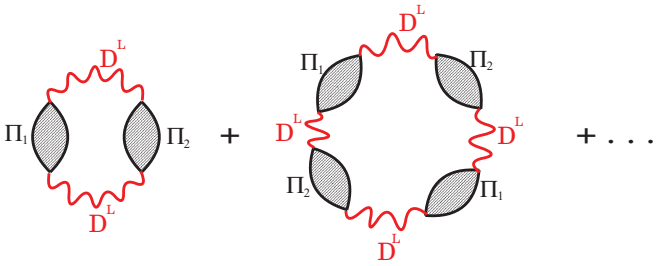

FIG. 2. (Color online) Interobject fluctuation diagrams in terms of current-current response functions.

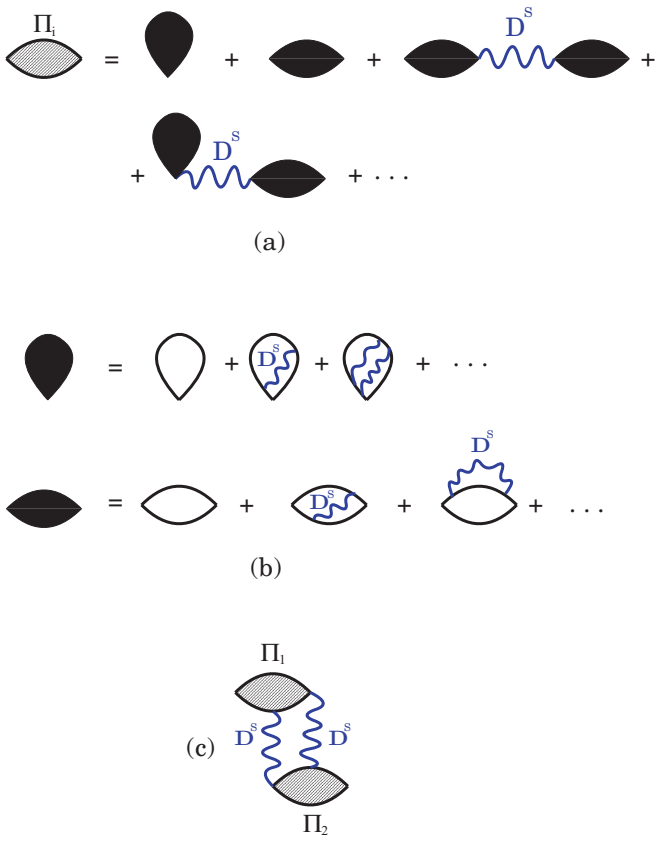

FIG. 3. (Color online) (a) Expansion of the current-current response function in terms of D^S; (b) irreducible polarizabilities; (c) two-photon exchange diagram.

the next higher order term is $\mathbf{\Theta}_4 = \mathbf{\Theta}_2\mathbf{D}^0\mathbf{\Theta}_2$, and so on. Hence, the free-energy shift can be written as

$$F - F_0 = -k_B T \sum_k{}' \mathrm{Tr}\left\{\frac{1}{2}\,\mathbf{\Pi}_1\mathbf{D}^0\mathbf{\Pi}_2\mathbf{D}^0 + \frac{1}{4}\,\mathbf{\Pi}_1\mathbf{D}^0\mathbf{\Pi}_2\mathbf{D}^0\mathbf{\Pi}_1\mathbf{D}^0\mathbf{\Pi}_2\mathbf{D}^0 + \cdots\right\}. \quad (9)$$

By using $\ln(1-A) = -A - \frac{1}{2}A^2 - \frac{1}{3}A^3 - \cdots$, the matrix series in (9) can be written in a compact form

$$F - F_0 = k_B T \sum_k{}' \mathrm{Tr}\ \ln\{1 - \mathbf{\Pi}_1(i\omega_k)\mathbf{D}^0(i\omega_k) \times \mathbf{\Pi}_2(i\omega_k)\mathbf{D}^0(i\omega_k)\}, \quad (10)$$

where we have omitted writing spatial coordinates. The tensors $\mathbf{\Pi}_i$ and $\mathbf{D}^0$ are retarded current-current and photon propagators, respectively, which are here also matrices in real space. So, the trace operation and matrix multiplications correspond to summations over polarization μ and integration over spatial coordinates.

III. RETARDED INTERACTION BETWEEN METALLIC SLABS

We shall now apply this formalism to the interaction between two metallic slabs schematically presented in Fig. 4. Electron currents and densities are localized inside the regions $-L_1 < z < 0$ and $d < z < L_2 + d$, where z is the coordinate perpendicular to metallic surfaces.

Because of planar symmetry, the tensors $\mathbf{\Pi}_i$ and $\mathbf{D}^0$ can be Fourier transformed in the plane parallel to metallic surfaces and expression (10) becomes

$$F - F_0 = k_B T \sum_k{}' \int \frac{d\mathbf{Q}}{(2\pi)^2}\mathrm{Tr}_\mu\mathrm{Tr}_z \times \ln\{1 - \mathbf{\Pi}_1(i\omega_k,\mathbf{Q})\mathbf{D}^0(i\omega_k,\mathbf{Q}) \times \mathbf{\Pi}_2(i\omega_k,\mathbf{Q})\mathbf{D}^0(i\omega_k,\mathbf{Q})\}. \quad (11)$$

Photon self-energy matrices $\mathbf{\Pi}_i$, illustrated in Fig. 3(a), consist of contributions, shown in Fig. 3(b), where the lowest-order terms are

$$\hat{\mathbf{\Pi}}_i = \hat{\mathbf{\Pi}}_i^{\mathrm{dia}} + \hat{\mathbf{\Pi}}_i^{\mathrm{para}}, \qquad i = 1,2. \quad (12)$$

The diamagnetic term[30] is a function of the density profile $n(z)$ shown in Fig. 7:

$$\hat{\mathbf{\Pi}}^{\mathrm{dia}}(Q,i\omega_k,z,z') = -\frac{e^2}{mc}n(z)\delta(z-z')\hat{\mathbf{I}}, \quad (13)$$

where $\hat{\mathbf{I}}$ is the unit matrix. Paramagnetic contribution (current-current response matrix)[30] for the metallic slab has the form

$$\Pi_{\mu\nu}^{\mathrm{para}}(\mathbf{Q},i\omega_k,z,z') = -\frac{1}{c}\sum_{\mathbf{K}nm}\frac{f_n(\mathbf{K}) - f_m(\mathbf{K}+\mathbf{Q})}{i\hbar\omega_k + E_n(\mathbf{K}) - E_m(\mathbf{K}+\mathbf{Q})} \times j_{nm}^{\mu}(2\mathbf{K}+\mathbf{Q},z)\, j_{mn}^{\nu}(2\mathbf{K}+\mathbf{Q},z'), \quad (14)$$

where $E_n(\mathbf{K}) = E_n + \frac{\hbar^2K^2}{2m}$, E_n are quantized levels in the direction perpendicular to the metallic slab, and $f_n(\mathbf{K})$ is the Fermi-Dirac distribution. At $T = 0$, the Fermi-Dirac distribution is $f_n(\mathbf{K}) = \theta[E_F - E_n(\mathbf{K})]$, where E_F is the Fermi level. Current density producing the transition from state $\{n,\mathbf{K}\}$ to $\{m,\mathbf{K}+\mathbf{Q}\}$ is

$$\mathbf{j}_{nm}(2\mathbf{K}+\mathbf{Q},z) = \frac{e\hbar}{2im}\{i\phi_n(z)\phi_m(z)(2\mathbf{K}+\mathbf{Q}) + [\phi_n(z)\partial_z\phi_m(z) - \phi_m(z)\partial_z\phi_n(z)]\hat{\mathbf{z}}\}. \quad (15)$$

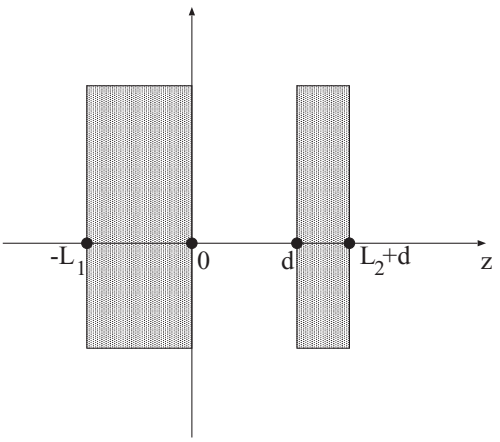

FIG. 4. Geometry of the system.

The two terms in (15) represent the currents parallel and perpendicular to the surface, respectively, and $\phi_n(z)$ are electronic wave functions in the z direction. The trace operation and matrix multiplication in (11) now correspond to summations over μ and integrations over z. We shall first perform the z integration. After expansion of the logarithm, Eq. (11) can be written as

$$F - F_0 = -k_B T \sum_k{}' \int \frac{d\mathbf{Q}}{(2\pi)^2} \mathrm{Tr}_\mu \left\{ \mathbf{A} + \frac{\mathbf{A}^2}{2} + \frac{\mathbf{A}^3}{3} + \cdots \right\}, \tag{16}$$

where

$$\begin{aligned} \mathbf{A} &= \int_{-L_1}^{0} dz_1 dz_2 \int_{d}^{L_2+d} dz_3 dz_4 \\ &\quad \times \mathbf{\Pi}_1(z_1,z_2)\,\mathbf{D}^0(z_2,z_3)\,\mathbf{\Pi}_2(z_3,z_4)\,\mathbf{D}^0(z_4,z_1) \\ &\equiv \mathrm{Tr}_z\{\mathbf{\Pi}_1 \otimes \mathbf{D}^0 \otimes \mathbf{\Pi}_2 \otimes \mathbf{D}^0\} \end{aligned} \tag{17}$$

is now the matrix with respect to polarization μ only, the symbol $\otimes$ represents the convolution in the coordinates z, and we have omitted writting $\mathbf{Q}$ and $i\omega_k$.

In the following, and also in Sec. III A, the expressions will be written as functions of real frequency. Explicit expression for the retarded free photon propagator $\mathbf{D}^0$ can be found in Refs. 30 or 32. If we choose the coordinate system so that $\mathbf{Q} = Q\mathbf{y}$, the free propagators of s- and p-polarized fields become

$$\mathbf{D}^0(Q\mathbf{y}, i\omega_k, z, z') = v_Q(\omega_k) \begin{cases} \mathbf{d}_+ e^{-\beta_k(z-z')}, & z > z' \\ \mathbf{d}_- e^{-\beta_k(z'-z)}, & z < z' \end{cases} \tag{18}$$

where $v_Q(\omega_k) = -\frac{2\pi Qc}{\omega_k^2}$ and we introduced the matrices

$$\mathbf{d}_\pm = \begin{bmatrix} d^s & 0 \\ 0 & \mathbf{d}_\pm^p \end{bmatrix}. \tag{19}$$

The component

$$d^s = -\frac{\omega_k^2}{Q\beta_k c^2} \tag{20}$$

corresponds to the s-polarized electromagnetic field and the matrices

$$\mathbf{d}_\pm^p = \begin{bmatrix} -\frac{\beta_k}{Q} & \mp i \\ \mp i & \frac{Q}{\beta_k} \end{bmatrix} \tag{21}$$

to the p-polarized electromagnetic field. The wave vector in the z direction is $\beta_k = \sqrt{\frac{\omega_k^2}{c^2} + Q^2}$. After using (18) and some manipulation, the expression (17) becomes

$$\mathbf{A} = e^{-2\beta_k d}\, \mathbf{P}_- \mathbf{P}_+, \tag{22}$$

where

$$\begin{aligned} \mathbf{P}_- &= v_Q(\omega_k) \int_{-L_1}^{0} dz_1 dz_2 e^{\beta_k(z_1+z_2)} \mathbf{\Pi}_1(z_1,z_2)\,\mathbf{d}_-, \\ \mathbf{P}_+ &= v_Q(\omega_k) \int_{0}^{L_2} dz_1 dz_2 e^{-\beta_k(z_1+z_2)} \mathbf{\Pi}_2(z_1,z_2)\,\mathbf{d}_+. \end{aligned} \tag{23}$$

$\mathbf{P}^\pm$ could be considered as **polarization propagators** on the left and right inner metallic surfaces (i.e., right surface of the left slab and left surface of the right slab), respectively.

A. Connection with surface polariton propagators

Now we shall show that the tensors $\mathbf{P}_\pm$ can be connected with the propagators of surface polaritons introduced in Ref. 30. The propagator of the electromagnetic field near some polarizable medium can be expressed as a series of Feynman diagrams, shown in Fig. 5(a). After the sum of polarization diagrams is recognized as the current-current response functions $\mathbf{\Pi}_\pm$ [already introduced in Figs. 3(a) and 3(b)], the propagator of the electromagnetic field can also be expressed as in Fig. 5(b).

The induced part of electromagnetic field can be calculated from the second term in Fig. 5(b). For example, the induced part of the electrical field at the right surface of the left slab can be calculated from the diagram in Fig. 6(a) and has the form[30]

$$\mathbf{E}_-^{\mathrm{ind}} = 2\pi Q\, \mathbf{D}_- \tag{24}$$

and, similarly at the left surface of the right slab from the diagram in Fig. 6(b),

$$\mathbf{E}_+^{\mathrm{ind}} = 2\pi Q\, \mathbf{D}_+ \tag{25}$$

where

$$\begin{aligned} \mathbf{D}_- &= v_Q(\omega_k) \int_{-L_1}^{0} dz_1 dz_2 \mathbf{d}_+ e^{\beta_k(z_1+z_2)} \mathbf{\Pi}_1(z_1,z_2)\,\mathbf{d}_-, \\ \mathbf{D}_+ &= v_Q(\omega_k) \int_{0}^{L_2} dz_1 dz_2 \mathbf{d}_- e^{-\beta_k(z_1+z_2)} \mathbf{\Pi}_2(z_1+d,z_2+d)\,\mathbf{d}_+ \end{aligned} \tag{26}$$

are now **propagators of surface polaritons** on the left and right inner metallic surfaces, respectively.

Comparing (26) and definitions (23), we get the connection

$$\begin{aligned} \mathbf{D}_- &= \mathbf{d}_+ \mathbf{P}_-, \\ \mathbf{D}_+ &= \mathbf{d}_- \mathbf{P}_+. \end{aligned} \tag{27}$$

By using (27), we can express $\mathbf{P}_\pm$ in terms of $\mathbf{D}_\pm$. Hence, as we know that $\mathbf{D}_\pm$ can be divided into s and p blocks[30] [as $\mathbf{D}^0$ in (18)–(21)],

$$\mathbf{D}_\pm = \begin{bmatrix} D_\pm^s & 0 \\ 0 & \mathbf{D}_\pm^p \end{bmatrix}, \tag{28}$$

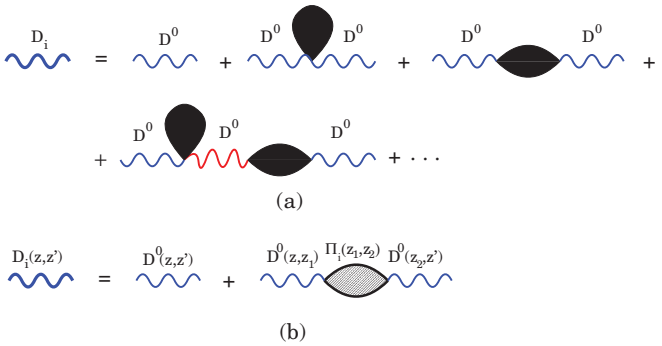

FIG. 5. (Color online) Propagators of the electromagnetic fields.

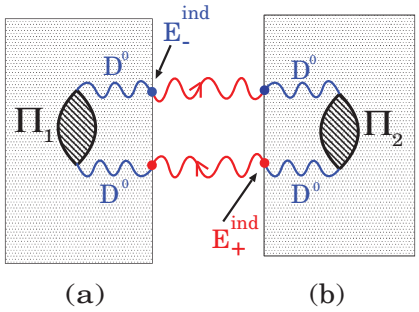

FIG. 6. (Color online) Feynman diagrams that represent induced electrical fields on (a) left and (b) right inner metal surfaces.

where

$$\mathbf{D}_{\pm}^{p}=\begin{bmatrix} D_{yy}^{\pm} & D_{yz}^{\pm} \\ D_{zy}^{\pm} & D_{zz}^{\pm} \end{bmatrix}. \tag{29}$$

This is also valid for $\mathbf{P}_{\pm}$. So, for s polarization, by using (20), we get

$$P_{\pm}^{s}=-\frac{Q\beta_k c^2}{\omega_k^2}\,D_{\pm}^{s}. \tag{30}$$

For p polarization, the procedure is not so straightforward because $\det\mathbf{d}_{\pm}^{p}=0$, and $\mathbf{P}_{\pm}^{p}$ can not be obtained from $\mathbf{D}_{\pm}^{p}$ directly by matrix inversion. Physically this means that the induced polarization $\mathbf{P}_{\pm}^{p}$ is not uniquely determined by external electrical field $\mathbf{D}_{\pm}^{p}$, i.e., there is some freedom in determining $\mathbf{P}_{\pm}^{p}$ from $\mathbf{D}_{\pm}^{p}$. Of course, the electrical field is always uniquely determined by polarization. Nevertheless, by taking into account these two facts, we have to solve directly the system of equations for p polarization (27), and we get

$$\mathbf{P}_{\pm}^{p}=\mathbf{a}^{\pm}\mathbf{D}_{\pm}^{p}, \tag{31}$$

where

$$\mathbf{a}^{\pm}=\begin{bmatrix} -\frac{Q}{\beta_k} & \pm i\frac{Q}{\beta_k}C_{\pm} \\ 0 & C_{\pm} \end{bmatrix} \tag{32}$$

and where arbitrariness of determining $\mathbf{P}_{\pm}^{p}$ from $\mathbf{D}_{\pm}^{p}$ is introduced through real arbitrary constants $C_{\pm}$.

By using (30) and (31), Eq. (22) becomes

$$\mathbf{A}=\begin{bmatrix} \frac{Q^2\beta_k^2c^4}{\omega_k^4}\,D_{-}^{s}D_{+}^{s} & 0 \\ 0 & \mathbf{a}^{-}\mathbf{D}_{-}^{p}\mathbf{a}^{+}\mathbf{D}_{+}^{p} \end{bmatrix} e^{-2\beta_k d} \tag{33}$$

and the trace in (16) can be written in the compact form (as before)

$$\mathrm{Tr}_{\mu}\ln\{1-\mathbf{A}\}. \tag{34}$$

In Sec. III B, we show that the free-energy shift can be separated into $s-$ and p-polarized parts for a general case, i.e., without the specific choice of the coordinate system $\mathbf{Q}=Q\mathbf{y}$ used in this section.

B. Separation of s- and p-polarized contributions

In the previous section, we considered the situation wherein the electromagnetic wave was propagated in the $\mathbf{Q}=Q\mathbf{y}$ direction when the tensors $\mathbf{d}_{\pm}$, $\mathbf{D}_{\pm}$, and $\mathbf{P}_{\pm}$ can be separated into s and p blocks. However, in (34), electromagnetic waves propagating in all $\mathbf{Q}$ directions contribute, so we have to justify this separation in (34) for general $\mathbf{Q}$. Our system is isotropic in the (x,y) plane and the tensors that describe propagation in different directions can be connected by using rotation operation in the plane perpendicular to the z axis

$$\mathbf{R}(\theta)=\begin{bmatrix} \cos\theta & \sin\theta & 0 \\ -\sin\theta & \cos\theta & 0 \\ 0 & 0 & 1 \end{bmatrix}.$$

For example, if θ denotes the angle between two directions of propagation $Q\mathbf{y}$ and $\mathbf{Q}$, with $|\mathbf{Q}|=Q$, the relation between the tensors $\mathbf{D}(Q\mathbf{y})$ and $\mathbf{D}(\mathbf{Q})$ is

$$\mathbf{D}(\mathbf{Q})=\mathbf{R}^{T}(\theta)\mathbf{D}(Q\mathbf{y})\mathbf{R}(\theta), \tag{35}$$

which leads to

$$\mathrm{Tr}_{\mu}\mathbf{D}(\mathbf{Q})=\mathrm{Tr}_{\mu}\{\mathbf{R}^{T}(\theta)\mathbf{D}(Q\mathbf{y})\mathbf{R}(\theta)\}=\mathrm{Tr}_{\mu}\mathbf{D}(Q\mathbf{y}).$$

Therefore, after choosing $Q\mathbf{y}$ as the referent direction, the contributions from all other directions of propagation are the same as in (33) and (34). Therefore, (34) can be inserted in (16) and ΔF can be divided into s and p parts:

$$F-F_0=\sum_{i=s,p}\Delta F_i, \tag{36}$$

where

$$\Delta F_s=k_{\mathrm{B}}T\sum_{k=0}{}'\int\frac{d\mathbf{Q}}{(2\pi)^2}\ln\left\{1-e^{-2\beta_k d}\,\frac{Q^2\beta_k^2c^4}{\omega_k^4}\,D_{-}^{s}D_{+}^{s}\right\} \tag{37}$$

and

$$\Delta F_p=k_{\mathrm{B}}T\sum_{k=0}{}'\int\frac{d\mathbf{Q}}{(2\pi)^2}\mathrm{Tr}_{\mu}\ln\{1-e^{-2\beta_k d}\mathbf{a}^{-}\mathbf{D}_{-}^{p}\mathbf{a}^{+}\mathbf{D}_{+}^{p}\}. \tag{38}$$

In (38), all tensors are now 2×2 matrices and $\mu=y,z$. Matrices $\mathbf{a}_{\pm}$ have the explicit form (32). Calculation of the surface polariton propagators $\mathbf{D}_{\pm}$ is described in Ref. 30, and expressions in the long-wavelength limit can be found in Ref. 32.

One would like to express the logarithm in (38) in terms of scalars rather than in terms of matrices, as, for example, in the s-polarized case, where each of the two scalars $D_{\pm}^{s}$ contains all spectral properties of the corresponding slab. This calculation is described in the Appendix. Hence, s and p contributions to the Casimir free energy at finite temperature can be rewritten in the final form as

$$\Delta F_s=k_{\mathrm{B}}T\sum_{k=0}{}'\int\frac{d\mathbf{Q}}{(2\pi)^2}\ln\{1-e^{-2\beta_k d}R_{-}^{s}R_{+}^{s}\} \tag{39}$$

and

$$\Delta F_p=k_{\mathrm{B}}T\sum_{k=0}{}'\int\frac{d\mathbf{Q}}{(2\pi)^2}\ln\{1-e^{-2\beta_k d}R_{-}^{p}R_{+}^{p}\}, \tag{40}$$

where

$$R_{-}^{s}=-\frac{Q\beta_k c^2}{\omega_k^2}\,D_{xx}^{s-},\quad R_{+}^{s}=-\frac{Q\beta_k c^2}{\omega_k^2}\,D_{xx}^{s+}, \tag{41}$$

$$R_-^p = \frac{Q}{\beta_k} D_{yy}^{p\,-}, \quad R_+^p = \frac{Q}{\beta_k} D_{yy}^{p\,+}. \tag{42}$$

Formally, similar expressions were obtained by Lifshitz[14] and by Abrikosov, Gorkov, and Dzyaloshinski a long time ago,[13] but they all treated metallic slabs using a local dielectric function. In Sec. IV B, we show that $R_-^{s,p}$ and $R_+^{s,p}$ in the long-wavelength limit correspond to the reflection coefficients $r_\pm^{s,p}$ on the left and right inner metallic surfaces.

The results (39)–(42) for the Casimir energy between two metallic slabs are beautifully simple and at the same time very powerful. Casimir energy is expressed directly in terms of two components of the polariton propagator matrix calculated for each of the slabs separately, without restriction to a specific response mechanism.

IV. DISCUSSION OF THE RESULTS

Expressions (39) and (40) for the electronic contribution to the Casimir free energy given in terms of generalized reflectivities (or polariton propagators) (41) and (42) are, in principle, exact provided that we describe the electronic response in a satisfactory approximation while other fluctuation mechanisms remain to be included in some other, usually phenomenological, way. In this section, we first show that these expressions reduce to the well-known results in the nonretarded and zero-temperature limits (where one recovers the usual van der Waals energies), and in the long-wavelength limit. These considerations are generally valid and do not depend on the assumed electronic response.

The level of accuracy of our calculations depends on the choice of the approximation that we use for the calculation of the electronic response. We use the jellium model and calculate self-consistent electronic wave functions in the LDA. To obtain the response functions, we use RPA, i.e., taking into account only the first terms in the expansions in Fig. 3(b).

A. Electrostatic zero-temperature limit and van der Waals interaction

Before proceeding with the calculation of the Casimir free energies (39) and (40), we show that these expressions reduce to the correct nonretarded ($c \to \infty$) and zero-temperature ($T \to 0$) limit, as well as to the standard Lifshitz result when nonlocality of response is neglected in the long-wavelength limit.

Transition to zero temperature is straightforward. Namely, because of

$$k_B T \sum_{\omega_k = 0} \to \hbar \int_0^\infty \frac{d\omega}{2\pi},$$

all we have to do is to substitute the summation over discrete frequencies in (39) and (40) by the integration over continuous frequencies. Also, the free-energy shift becomes the energy shift

$$F - F_0 \to E - E_0 = \Delta E_s + \Delta E_p.$$

Propagators in (39) and (40) remain unchanged except that they become functions of continuous frequency $i\omega$.

From (41), it appears that $R_\pm^s$ is proportional to c^2, but it is easy to show that $D_{xx}^{s\pm}$ is proportional to $1/c^4$, so $R_\pm^s$ actually vanishes quadratically with c, which means that, in the nonretarded limit, $\Delta E_s = 0$ and we only need to consider the p-polarized contribution.

To do this, we first need to transform the integration in (40) to the real frequencies. $R_\pm^p$ in (40) are real functions of imaginary frequency $i\omega$, so ΔE_p is real. After substituting $u = i\omega$, closing the integration contour in the first quadrant of the complex ω plane, and using the fact that $R_\pm^p$ are analytic functions in the upper ω plane, (40) becomes

$$\Delta E_p = \hbar \ \mathrm{Im} \int \frac{d\mathbf{Q}}{(2\pi)^2} \int_0^\infty \frac{d\omega}{2\pi} \ln\{1 - e^{2i\beta d} R_-^p R_+^p\}, \tag{43}$$

where $R_\pm^p$ are complex functions of real frequency, exactly as they appear in (A12).

In order to find the $c \to \infty$ limit of $D_{\mu\nu}^{p\pm}$ in (A12), we first relate the propagator of the electromagnetic field $\mathbf{D}$ to the propagator of the screened Coulomb interaction W in the nonretarded limit using the result[30]

$$\lim_{c\to\infty} \frac{\omega^2}{c} D_{\mu\nu}^{p,\mathrm{ind}}(Q,\omega,z,z') = \left[i\mathbf{Q} + \mathbf{z}\frac{\partial}{\partial z} \right]_\mu \left[i\mathbf{Q} - \mathbf{z}\frac{\partial}{\partial z'} \right]_\nu W^{\mathrm{ind}}(Q,\omega,z,z'). \tag{44}$$

Obviously, we shall apply (44) to $\mu, \nu = y, z$ only.Furthermore, the induced part of W can be related to the propagator of surface excitations $D(\mathbf{Q},\omega)$,[31,33–36]

$$W_\pm^{\mathrm{ind}}(\mathbf{Q},\omega,z,z') = \frac{2\pi}{Q} D_\pm(\mathbf{Q},\omega)\, e^{\pm Q(z+z')}, \tag{45}$$

where $+$ and $-$ correspond to the right and left surfaces, respectively. After inserting (45) in (44), with $\mathbf{Q} = Q\mathbf{y}$, performing the derivatives, and inserting $z = z' = 0$, with the help of (24), (25), and (A12) with $\alpha \to -i$, we can easily show that

$$R_\pm^p = -D_\pm(\mathbf{Q},\omega) \tag{46}$$

so that the expression (43) for the van der Waals energy becomes

$$\Delta E_p = \hbar \ \mathrm{Im} \int \frac{d\mathbf{Q}}{(2\pi)^2} \int_0^\infty \frac{d\omega}{2\pi} \times \ln\{1 - e^{-2Qd} D_+(\mathbf{Q},\omega) D_-(\mathbf{Q},\omega)\}, \tag{47}$$

which is exactly Eq. (23) in Ref. 31. Comparison with (40) shows that $R_\pm^p$ in the $c \to \infty$ limit play the role of surface excitation propagators $D_\pm$, including effects of nonlocality as discussed in Ref. 31.

B. Long-wavelength (local) limit

Now we want to compare our results (39) and (40) with the standard results for the Casimir force obtained by the usual electromagnetic field matching procedure, which is possible when the media have sharp boundaries and are described by local dielectric functions. Tensors $\mathbf{D}_\pm$ in (37) and (38) have exact physical meaning as expressed in (24) and (25), where $\mathbf{E}_\pm^{\mathrm{ind}}$ is the induced electrical field produced by the unit point dipole placed at the right (left) inner surface, assuming that

the slabs are infinitely separated, i.e., $d \to \infty$. Expressions for induced electrical fields in the long-wavelength limit are easily obtainable and the transition to $Q \to 0$ is straightforward. For example, compact expressions for $\mathbf{E}_{\pm}^{\mathrm{ind}}$ even for arbitrary planar configurations can be found in Ref. 32. After inserting Eq. (2.22) of Ref. 32 into (24) and (25), we get

$$D_{\pm}^{s} \equiv D_{xx}^{s\pm} = -\frac{\omega_k^2}{\beta_k Q c^2} r_{\pm}^{s} \tag{48}$$

and

$$\mathbf{D}_{\pm}^{p} = r_{\pm}^{p} \begin{bmatrix} \frac{\beta_k}{Q} & \pm i \\ \mp i & \frac{Q}{\beta_k} \end{bmatrix}, \tag{49}$$

where $r_{-}^{s,p}$ are reflection coefficients for s- and p-polarized electromagnetic plane waves incident on the planar configuration placed in $z < 0$, and $r_{+}^{s,p}$ are reflection coefficients for s- and p-polarized electromagnetic plane waves incident on the planar configuration placed in $z > d$. These coefficients are obtained using the boundary conditions at sharp metallic surfaces and do not include dispersion. After inserting (48) into (41) and matrix elements $D_{yy}^{p\pm}$ of (49) into (A12), we get

$$R_{\pm}^{s} \to r_{\pm}^{s}, \quad R_{\pm}^{p} \to r_{\pm}^{p}, \tag{50}$$

which again shows that $R_{\pm}^{p}$ have the roles of surface reflectivities. After inserting (50) into (39) and (40), we obtain, as expected, the local expressions for the Casimir free energy in terms of reflection coefficients

$$\Delta F_{s}^{\mathrm{local}} = k_{\mathrm{B}} T \sum_{k=0}{}' \int \frac{d\mathbf{Q}}{(2\pi)^2} \ln\{1 - r_{-}^{s} r_{+}^{s}\, e^{-2\beta_k d}\}, \tag{51}$$

$$\Delta F_{p}^{\mathrm{local}} = k_{\mathrm{B}} T \sum_{k=0}{}' \int \frac{d\mathbf{Q}}{(2\pi)^2} \ln\{1 - r_{-}^{p} r_{+}^{p}\, e^{-2\beta_k d}\}. \tag{52}$$

C. Diamagnetic and paramagnetic contributions

Photon self-energy terms shown in Fig. 2 and their lowest-order terms given by Eqs. (12)–(15) deserve some comments concerning their specific physical roles in the Casimir energy.

The diamagnetic term represents local density fluctuations [including their higher-order corrections, screening, etc., as shown in Fig. 3(b)], and it has its counterpart in classical electrodynamics. When the electronic response is described in the local approximation, e.g., by the local dielectric function $\epsilon_i(\omega)$ for the medium i, this corresponds to the sharp (steplike) charge-density profile at the surface, and standard EM field matching procedures can be applied. Attempts to combine arbitrary density profiles with EM boundary conditions lead to unavoidable difficulties, requiring additional boundary conditions or some other approximation. As our starting point is the microscopic description of electrons in terms of their wave functions, we are able, by using (13), to include diamagnetic contributions to the Casimir energy exactly, with the electron density profile calculated from first principles.

The paramagnetic term in Fig. 3(b) and Eq. (14) represents nonlocal current-current fluctuations, i.e., intraband and interband electronic transitions, and here it was included in the proper nonlocal description of electrons in a metallic slab.

As is obvious, e.g., from Figs. 3(a) and 3(b), these two contributions can not be separated since each one is modified by the self-energy terms that combine both processes. However, in our analysis in Sec. IV E, we show that, in a specific application, these two physically distinct contributions to the Casimir energy can be, to a very good approximation, identified and discussed separately.

To clarify the origin and the role of each contribution to the photon self-energy tensor $\mathbf{\Pi}$, it is useful to explore how it is related to the nonlocal dielectric tensor $\boldsymbol{\epsilon}$. For a polarizable system of arbitrary symmetry described by the nonlocal dielectric tensor $\boldsymbol{\epsilon}$ in the linear response approximation, electric field $\mathbf{E}$ and electric displacement $\mathcal{D}$ are related as

$$\mathcal{D} = \boldsymbol{\epsilon} \otimes \mathbf{E}, \tag{53}$$

where $\otimes$ represents matrix multiplication and convolution in real space. The electric field in the presence of a point dipole $\mathbf{p}$ then can be obtained by solving the equation[30,32]

$$\left\{\nabla \times \nabla \times \delta(\mathbf{r} - \mathbf{r}_1)\hat{\mathbf{I}} - \frac{\omega^2}{c^2}\hat{\boldsymbol{\epsilon}}(\mathbf{r},\mathbf{r}_1,\omega)\right\} \otimes \mathbf{E}(\mathbf{r}_1,\mathbf{r}',\omega) = 4\pi \frac{\omega^2}{c^2}\delta(\mathbf{r} - \mathbf{r}')\mathbf{p}, \tag{54}$$

where $\hat{\mathbf{I}} = \mathbf{xx} + \mathbf{yy} + \mathbf{zz}$ is the unit dyadic, and the variable in all differential operators is $\mathbf{r}$. On the other hand, using the Dyson equation for the photon propagator

$$\mathbf{D} = \mathbf{D}_0 + \mathbf{D}_0 \otimes \mathbf{\Pi} \otimes \mathbf{D}$$

and the relation[30]

$$\mathbf{E}(\mathbf{r},\mathbf{r}',\omega) = \frac{\omega^2}{c}\mathbf{D}(\mathbf{r},\mathbf{r}',\omega)\mathbf{p},$$

we can obtain the Dyson equation for the electric field

$$\mathbf{E} = \mathbf{E}_0 + \mathbf{D}_0 \otimes \mathbf{\Pi} \otimes \mathbf{E}. \tag{55}$$

Acting on both sides with the operator $\nabla \times \nabla \times -\frac{\omega^2}{c^2}$, by using Eq. (54) for vacuum ($\boldsymbol{\epsilon} = \mathbf{1}$) and the differential equation for free photon propagator

$$\left\{\nabla \times \nabla \times -\frac{\omega^2}{c^2}\right\} \mathbf{D}_0(\mathbf{r}_1,\mathbf{r}',\omega) = \frac{4\pi}{c}\delta(\mathbf{r} - \mathbf{r}')\hat{\mathbf{I}}, \tag{56}$$

we get

$$\left\{\nabla \times \nabla \times \delta(\mathbf{r} - \mathbf{r}_1)\hat{\mathbf{I}} - \frac{\omega^2}{c^2}\left[\delta(\mathbf{r} - \mathbf{r}_1)\hat{\mathbf{I}} + \frac{4\pi c}{\omega^2}\mathbf{\Pi}(\mathbf{r},\mathbf{r}_1,\omega)\right]\right\} \otimes \mathbf{E}(\mathbf{r}_1,\mathbf{r}',\omega) = 4\pi \frac{\omega^2}{c^2}\delta(\mathbf{r} - \mathbf{r}')\mathbf{p}. \tag{57}$$

By comparing (54) and (57), we can obtain the general relationship between the dielectric tensor and the photon self-energy $\hat{\mathbf{\Pi}}$:

$$\hat{\boldsymbol{\epsilon}}(\mathbf{r},\mathbf{r}',\omega) = \delta(\mathbf{r} - \mathbf{r}')\hat{\mathbf{I}} + \frac{4\pi c}{\omega^2}\hat{\mathbf{\Pi}}(\mathbf{r},\mathbf{r}',\omega). \tag{58}$$

After Fourier transforming and substituting(12)–(14), we get

$$\epsilon_{\mu\nu}(z,z',Q,\omega) = \epsilon^{L}(z,\omega)\delta(z - z')\delta_{\mu\nu} + \epsilon_{\mu\nu}^{T}(z,z',Q,\omega), \tag{59}$$

where

$$\epsilon^L(z,\omega) = 1 - \frac{\omega_p^2(z)}{\omega^2}, \tag{60}$$

$$\epsilon^T_{\mu\nu}(z,z',Q,\omega) = \frac{4\pi c}{\omega^2}\Pi^{\rm para}_{\mu\nu}(Q,\omega,z,z'), \tag{61}$$

and $\omega_p^2(z) = \frac{4\pi e^2 n(z)}{m}$ is the local plasma frequency. ϵ^L is what is usually called the longitudinal dielectric function, in the long-wavelength limit. Here, it is obvious that ϵ^L is the local part of the dielectric function related to the general (i.e., continuous) density profile. It is derived from $\Pi^{\rm dia}_{\mu\nu}$ and represents the charge-density polarization. $\epsilon^T_{\mu\nu}$ is the correction to ϵ^L that contains longitudinal and transverse components and, in the long-wavelength (local) limit, it becomes longitudinal as well. From (61), we can see that $\epsilon^T_{\mu\nu}$ is proportional to $\Pi^{\rm para}_{\mu\nu}$ and represents polarization originating from electron-hole transitions. In other words, $\epsilon^T_{\mu\nu}$ is the nonlocal part of the dielectric function and the nonlocality is taken into account through exact calculation instead of being added through some parametrized procedure. As we can see from Ref. 30 (Sec. II A), the tensor $\Pi^{\rm para}_{\mu\nu}$ is not purely transverse, but it consists of diagonal (longitudinal) and nondiagonal (transverse) parts, and the transverse part vanishes in the long-wavelength limit. From this discussion, it is obvious that there is no direct way to connect the expressions (59)–(61) with the transverse and longitudinal dielectric functions in a homogeneous medium.

In the calculation of the Casimir free energy, we can, in principle, use the dielectric tensors (59)-(61) or the polarization propagator $\mathbf{\Pi}$. Also, to investigate the influence of the nonlocal effects and density profile on the Casimir free energy, we compare our nonlocal results with those obtained by performing the same calculation using a local Drude dielectric function

$$\epsilon(\omega) = 1 - \frac{\omega_p^2}{\omega(\omega + i\eta)}. \tag{62}$$

The plasmon frequency is $\omega_p^2 = \frac{4\pi e^2 n^+}{m}$ inside the slab and $\omega_p^2 = 0$ outside the slab, n^+ is the positive background density, while η is the damping parameter that reflects the dissipation inside the slabs.

D. Computational method

To apply this theory to a specific physical problem, we need to rewrite some of the expressions used for the local and nonlocal calculations of Casimir free energy in the form more suitable for the numerical calculations. Propagators of surface polaritons (26) are proportional to the induced part of the electromagnetic field propagator $\mathbf{D}^{\rm ind}_{\pm}(\mathbf{Q},\omega,z=0,z'=0)$:[30]

$$\mathbf{D}_{\pm} = \frac{1}{v_Q(\omega_k)}\mathbf{D}^{\rm ind}_{\pm}(\mathbf{Q},i\omega_k,z=0,z'=0), \tag{63}$$

where $z=0$ is the position of the right electron density edge. By combining (41), (42), and (63) and using $\hbar = m = c = e = 1$ unit system, the generalized reflectivities can be numerically calculated by using

$$R^s_{\pm} = \frac{\beta_k^2}{2\pi\gamma^2}D^{{\rm ind},\pm}_{xx}(\mathbf{Q},i\omega_k,z=0,z'=0), \tag{64}$$

$$R^p_{\pm} = -\frac{\omega_k^2}{2\pi\beta_k^2}D^{{\rm ind},\pm}_{yy}(\mathbf{Q},i\omega_k,z=0,z'=0), \tag{65}$$

where $\beta_k = \sqrt{\gamma^2\omega_k^2 + Q^2}$ and $\gamma = \frac{e^2}{\hbar c}$ is the fine-structure constant. The electromagnetic field-tensor components $D^{\rm ind}_{xx}$ and $D^{\rm ind}_{yy}$ can be obtained by solving the Dyson equation for each slab

$$\begin{aligned}\hat{\mathbf{D}}(\mathbf{Q},i\omega_k,z,z') = \hat{\mathbf{D}}^0(\mathbf{Q},i\omega_k,z,z') + \hat{\mathbf{D}}^0(\mathbf{Q},i\omega_k,z,z_1)\\ \otimes\hat{\mathbf{\Pi}}^{\rm dia}(\mathbf{Q},i\omega_k,z_1,z_2)\otimes\hat{\mathbf{D}}(\mathbf{Q},i\omega_k,z_2,z')\\ + \hat{\mathbf{D}}^0(\mathbf{Q},i\omega_k,z,z_1)\otimes\hat{\mathbf{\Pi}}^{\rm para}(\mathbf{Q},i\omega_k,z_1,z_2)\\ \otimes\hat{\mathbf{D}}(\mathbf{Q},i\omega_k,z_2,z'),\end{aligned} \tag{66}$$

where the electron density (current) is located in the interval $z\in(-L,0)$ and $\otimes = \int_{-L}^{0} dz$ denotes the convolution in the z coordinate. Because the procedure is the same for both slabs, for clarity we omit the symbol $\pm$ in the superscripts of the tensors. By choosing $\mathbf{Q} = Q\mathbf{y}$, components of the free photon propagator become

$$D^0_{xx}(Q,i\omega_k,z,z') = \frac{2\pi}{c\beta_k}e^{-\beta_k|z-z'|}, \tag{67}$$

$$D^0_{yy}(Q,i\omega_k,z,z') = \frac{2\pi c\beta_k}{\omega_k^2}\,e^{-\beta_k|z-z'|}, \tag{68}$$

$$D^0_{zz}(Q,i\omega_k,z,z') = \frac{4\pi c}{\omega_k^2}\delta(z-z') - \frac{2\pi cQ^2}{\beta_k\omega_k^2}\,e^{-\beta_k|z-z'|}, \tag{69}$$

and

$$\begin{aligned}D^0_{yz}(Q,i\omega_k,z,z') &= D^0_{zy}(Q,i\omega_k,z,z')\\ &= \frac{2\pi icQ}{\omega_k^2}{\rm sgn}(z-z')\,e^{-\beta_k|z-z'|}.\end{aligned} \tag{70}$$

Photon self-energies [needed to solve (66)] are explicitly given by expressions (13) and (14), and a solution method is described in Ref. 30. After we solve the equation (66), the induced part of the photon propagator can be obtained as

$$\begin{aligned}\hat{\mathbf{D}}^{\rm ind}(\mathbf{Q},i\omega_k,z=0,z'=0) = \hat{\mathbf{D}}(\mathbf{Q},i\omega_k,z=0,z'=0)\\ -\hat{\mathbf{D}}^0(\mathbf{Q},i\omega_k,z=0,z'=0).\end{aligned} \tag{71}$$

By inserting xx and yy components of (71) first into (64) and (65) and then into (39) and (40), and performing a simple frequency summation and wave-vector integration, we get the Casimir free energy.

For the local calculation of the Casimir free energy, we use expressions (51) and (52) and the reflectivity coefficients taken from Ref. 32:

$$r^{s,p}_{\pm} = \frac{r^{s,p}_{v/m}}{D_{s,p}}(1 - e^{-2\beta'_k d}), \tag{72}$$

where $D_{s,p} = 1 - [r^{s,p}_{v/m}]^2 e^{-2\beta'_k d}$ and

$$r^s_{v/m} = \frac{\beta_k - \beta'_k}{\beta_k + \beta'_k}, \quad r^p_{v/m} = \frac{\epsilon(\omega_k)\beta_k - \beta'_k}{\epsilon(\omega_k)\beta_k + \beta'_k} \tag{73}$$

are the reflectivity coefficients for s- and p-polarized electromagnetic waves incident on the vacuum (metal) interface. Here, $\beta'_k = \sqrt{\gamma^2\epsilon(\omega_k)\omega_k^2 + Q^2}$, the thickness d of the slab is chosen to correspond to the jellium background thickness, and the dielectric function is given by (62). For the plasmon

frequency, we have chosen $\omega_p = 9.07$ eV, which corresponds to the jellium bulk plasma frequency of silver, while the damping parameter needs to be determined phenomenologically by fitting the results for the reflection coefficients to the experimental data, and for silver it is $\eta = 100$ meV.[37]

E. Application to silver films

To demonstrate the scope of our theory, we apply it to investigate Casimir energy between two silver slabs. The electronic structure of silver films will be described using a jellium model. For a silver metallic slab, we choose a positive background of thickness $31a_0$ and the density that corresponds to $r_s = 3$. The self-consistently calculated work function is $\phi = 3.51$ eV, and there are seven occupied states. The corresponding density profile is shown by a (thick solid) line in Fig. 7.

The conductivities inside each metallic slab are calculated using these eigenstates and density, as well as the previously described RPA method, which means that we do not include any dissipation that would lead to finite conductivity. In order to describe more realistic metallic slabs, all ohmic losses should be included, i.e., even though we have calculated the contribution of electron-hole excitations to a very high level of accuracy, there are other processes (phonons, impurities, etc.) that we have neglected.

The Drude model includes all dissipation mechanisms through the plasmon damping parameter η, which is determined phenomenologically by fitting the results for the reflection coefficients to the experimental data. This means that the Drude model calculations, even though relatively simple compared to our calculations, can give more realistic results for the Casimir energies since they include all the dissipation mechanisms, but they do not provide a way to distinguish among these mechanisms nor explore their individual influence on the Casimir force. Our formulation includes only collective and single-particle effects of electron-electron interaction, both included by means of a detailed, nonlocal calculation, exact within the model used to describe the response of the metallic slabs. The purpose of our calculations is not to obtain more accurate results than the ones obtained by the, e.g., Drude model, but to compare them with the ones obtained by the Drude model (with and without dissipation). This will give us information about the importance of low-energy electron-hole excitations.

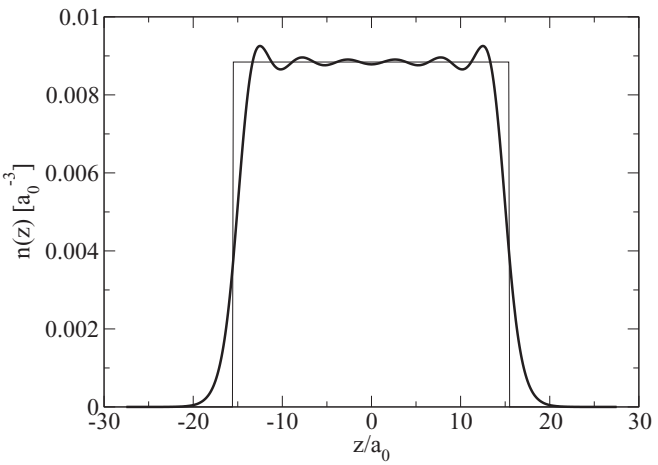

FIG. 7. Thin solid line: rectangular electronic density profile that corresponds to jellium edges. Thick solid line: LDA electron density profile. The corresponding parameters are presented in the text.

Our model enables us to evaluate selectively different contributions [diamagnetic, paramagnetic, s(TE), or p(TM)] to the Casimir energy. The results show that, e.g., if only diamagnetic contribution is included, it corresponds to a system without dissipation, i.e., with the system with infinite dc conductivity, and the results are the same as those obtained by the Drude model without dissipation ($\eta = 0$). On the other hand, the Casimir force obtained using a simple Drude dielectric function with realistic damping parameter is in excellent agreement with the one obtained using the experimental dielectric function[3,4,21] and with the one obtained from experiments at room temperature.[5] It means that the Drude model can provide a good description of the room-temperature Casimir force and also that inclusion of the paramagnetic contribution in our dielectric function can tell us exactly how much electron-hole pairs participate in this process.

To investigate this, we compare the Drude model without dissipation, our nonlocal calculations, and the Drude model with realistic damping. Figure 8 shows the calculated Casimir free energies as functions of separation between slabs at room temperature $T = 300$ K. The solid (black) lines represent results obtained from the Drude model with dissipation where $\eta = 100$ meV is taken from literature,[37] the dashed (red) lines represent the results of our nonlocal theory, i.e., calculated from the expressions (39)–(42), and the dotted (blue) lines represent results obtained from the Drude model without dissipation ($\eta = 0$). The left set of graphs shows the Casimir free energies at shorter separations (0.2–1 μm), while the right set shows Casimir free energies at larger separations (1.2–5 μm).

In all figures, we see a reduction of Casimir energies with respect to the calculation that does not include dissipation. This has been observed before,[3,4,21–23] where the calculations were performed using the local Drude models with and without dissipation, and it was concluded that dissipation is indeed responsible for the effects. Namely, the $k = 0$ term in expression (51) has a finite value if no dissipation is taken into account, while it is equal to zero as soon as any dissipation is included. This is also in agreement with our results in which we have shown that the effect results from the electron-hole excitations, which occur in the paramagnetic term.

The decomposition to s and p contributions shown in the four bottom graphs provides additional understanding. We see that the p contribution in all three models is almost the same. On the other hand, for the s mode at short separations, reduction due to the low-energy electron-hole excitations is almost half of the Drude reduction. At larger separations (especially as d approaches 5 μm), reduction due to this mechanism is negligible compared to all other dissipation mechanisms that cause the Drude model result to drop to zero at large separations.

This influences the total Casimir energy in a very delicate way. At large separations (3 μm $< d <$ 5 μm), the Drude result with dissipation is exactly half of the Drude result without dissipation. This is because, at such separations,

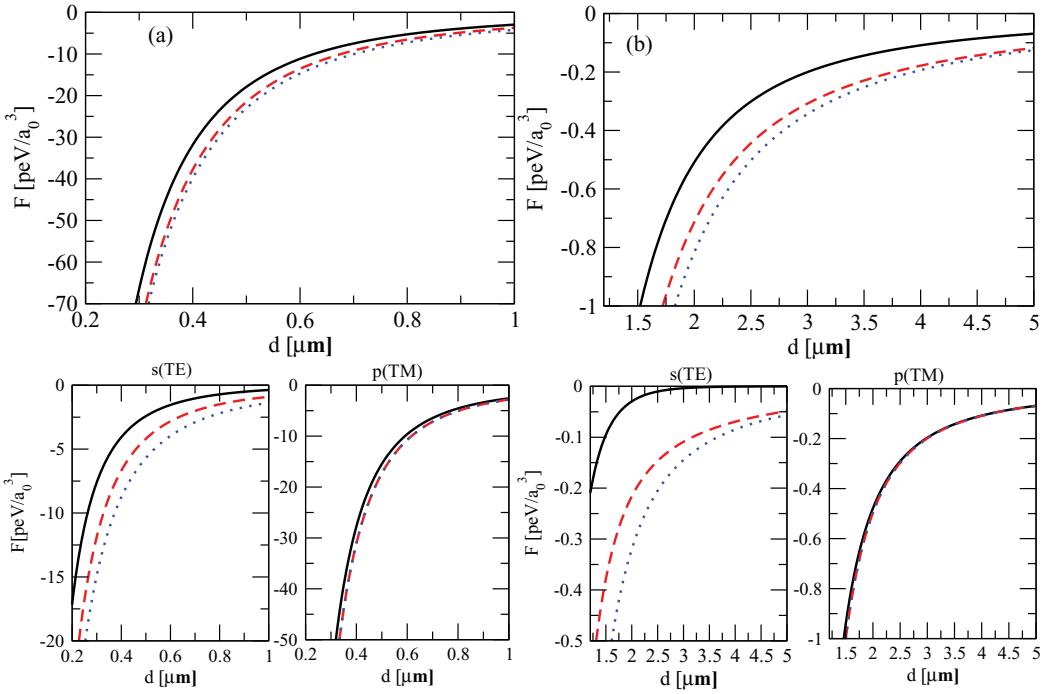

FIG. 8. (Color online) Casimir free energies for two silver slabs with thicknesses $31a_0$ at room temperature ($T = 300$ K) calculated in the jellium model, as a function of distance between the slabs. Solid (black) lines: Drude model with dissipation; dashed (red) lines: nonlocal calculation without dissipation; dotted (blue) lines: Drude model without dissipation. Graph (a) shows distances up to 1 μm while graph (b) shows distances from 1 to 5 μm. The four graphs in the bottom show s(TE) and p(TM) contributions of the Casimir energies of the graphs above them.

Drude reflectivities without dissipation behave like perfect metal reflectivities, i.e., s and p contributions are equal, and when dissipation is included, the s contribution drops to zero while the p contribution is not influenced. On the other hand, electron-hole pairs do not influence the s mode that much, and the total Casimir force at large separation is close to the result obtained by the Drude model without dissipation. Therefore, at large separations, the nonlocal effects are not important, while other dissipation mechanisms reduce the Casimir force exactly by a factor of 2.[4]

However, at smaller separations ($d < 1$ μm), the influence of nonlocality is not so unimportant since about $1/2$ of the total s reduction is caused by the dissipation originating from the nonlocal effects. To support this, we have performed careful analysis of the s reflectivity around $\omega = 0$ and found that this reduction is due to the low-energy intraband electron-hole excitations. They cause the s reflectivity to drop to zero for $\omega = 0$, while the excitation of the interband electron-hole pairs does not influence s reflectivities at all.

V. CONCLUSION

The results presented in this paper and discussed in Sec. IV show that we have developed a fully self-consistent nonlocal microscopic theory of the Casimir effect exactly within the used model. Diamagnetic, i.e., density fluctuations are treated microscopically and expressed in terms of the calculated electron density (instead of some externally introduced density and dielectric function). Another important feature is that the theory properly treats the paramagnetic contribution, including electron-hole excitations.

The main advantage of this contribution to the theory of Casimir energy is the method of calculating surface reflectivities, which includes dispersion and can be applied for smooth charge-density profiles, and is directly related to the surface polariton propagators.[30]

This formulation is applied to investigate the Casimir force between two silver slabs. As it is well known, treating metallic slabs as perfect conductors leads to incorrect results for the Casimir force, inconsistent with experiments, while a realistic description that includes dissipation (even through the simple Drude model) gives physically acceptable Casimir force. This is mainly because dissipation cancels the s-polarized contribution and the Casimir force drops to one-half of the perfect metal result.

In our calculation, we only included the electronic collective and single-particle excitations, neglecting other physical processes, and showed that, at large (macroscopic) separations ($d > 5$ μm), the resulting Casimir force is the same as for the perfect metal case, which means that the low-energy electron-hole excitations are not important for large separations between the slabs. However, at smaller separations ($d < 1$ μm), our correction of the perfect metal result is definitely not negligible. The result presented here is that about $1/2$ of the total s reduction calculated by the Drude model caused by low-energy electron-hole excitations.

The relative insensitivity of the Casimir force to the precise shape of the response mechanism is easy to explain. The Casimir force is an integrated quantity and includes all possible fluctuations, so the contributions e.g., from the low-energy tail of the damped Drude plasmon and from the continuum of the

electron-hole pairs are difficult to distinguish. The situation, however, is different in the calculation of quantum friction,[38] where the response mechanism is exactly the same, but the excitation spectrum appears in the final state, so the above two cases can be easily distinguished.

ACKNOWLEDGMENTS

The authors are grateful to Pedro Miguel Echenique for the hospitality at DIPC where this work was finalized, and for useful discussions with E. Chulkov, V. Silkin, and M. S. Tomaš. One of us (V.D.) acknowledges the support of the University of the Basque Country and the Spanish Ministerio de Ciencia y Tehnologia.

APPENDIX: CASIMIR FREE ENERGY IN TERMS OF GENERALIZED REFLECTIVITIES

We want to evaluate the trace in (38) and, specifically, the product of the matrices in the logarithm. We first notice that matrices $\mathbf{d}^p_\pm$ have linearly dependent rows

$$d^p_{\pm,z\mu} = \mp\alpha\, d^p_{\pm,y\mu}, \quad \mu = y,z \tag{A1}$$

where $\alpha = -i\frac{Q}{\beta_k}$. After inserting (A1) into (27), the matrices $\mathbf{D}^p_\pm$ become

$$\mathbf{D}^p_\pm = \begin{bmatrix} D^{p\,\pm}_{yy} & D^{p\,\pm}_{yz} \\ \pm\alpha\, D^{p\,\pm}_{yy} & \pm\alpha\, D^{p\,\pm}_{yz} \end{bmatrix}. \tag{A2}$$

By multiplying the two and two matrices and using $\mathrm{Tr}\ln\mathbf{A} = \ln\det\mathbf{A}$, the trace in (38) can be written as

$$\ln\det\{1 - \mathbf{MN}e^{-2\beta_k d}\}, \tag{A3}$$

where

$$\mathbf{M} = \begin{bmatrix} M_{yy} & XM_{zz} \\ \frac{1}{X}M_{yy} & M_{zz}, \end{bmatrix}, \quad \mathbf{N} = \begin{bmatrix} N_{yy} & YN_{zz} \\ \frac{1}{Y}N_{yy} & N_{zz}, \end{bmatrix}, \tag{A4}$$

$$\begin{aligned} M_{yy} &= -\alpha(\alpha C_- + i)D^{p\,-}_{yy},\ M_{zz} = -\alpha C_- D^{p\,-}_{yz}, \\ N_{yy} &= -\alpha(\alpha C_+ + i)D^{p\,+}_{yy},\quad N_{zz} = \alpha C_+ D^{p\,+}_{yz}, \end{aligned} \tag{A5}$$

and where $X = \frac{\alpha C_- + i}{C_-}$, $Y = -\frac{(\alpha C_+ + i)}{C_+}$. The determinants of the matrices $\mathbf{M}$ and $\mathbf{N}$ are equal to zero, as well as $\det\ \mathbf{MN}$, so after using

$$\ln\det(1 - \mathbf{A}) = \ln(1 - \mathrm{Tr}\mathbf{A} + \det\mathbf{A}),$$

(A3) becomes

$$\ln\left\{1 - \left[M_{yy} + \frac{X}{Y}M_{zz}\right]\left[N_{yy} + \frac{Y}{X}N_{zz}\right]e^{-2\beta_k d}\right\}. \tag{A6}$$

After inserting (A5), X, and Y in (A6), we get

$$\ln\{1 - e^{-2\beta_k d}\tilde{R}^p_-\tilde{R}^p_+\}, \tag{A7}$$

where

$$\tilde{R}^p_- = -\frac{\alpha C_- + i}{\alpha C_+ + i}R^p_-, \quad \tilde{R}^p_+ = -\frac{\alpha C_+ + i}{\alpha C_- + i}R^p_+$$

and

$$\begin{aligned} R^p_- &= \alpha\left[(\alpha C_+ + i)D^{p\,-}_{yy} - C_+ D^{p\,-}_{yz}\right], \\ R^p_+ &= \alpha\left[(\alpha C_- + i)D^{p\,+}_{yy} + C_- D^{p\,+}_{yz}\right]. \end{aligned} \tag{A8}$$

Because $\tilde{R}^p_\pm$ in (A7) appear in a product, the result obviously does not depend on the ratio between C_+ and C_-, so without losing the generality, we can put $C_+ = C_- = C$ and the logarithm (A7) can be written as

$$\ln\{1 - e^{-2\beta_k d}R^p_-R^p_+\}, \tag{A9}$$

where

$$\begin{aligned} R^p_- &= \alpha\left[(\alpha C + i)D^{p\,-}_{yy} - C D^{p\,-}_{yz}\right], \\ R^p_+ &= \alpha\left[(\alpha C + i)D^{p\,+}_{yy} + C D^{p\,+}_{yz}\right]. \end{aligned} \tag{A10}$$

Now, one can conclude that the result for the Casimir force depends on an arbitrary constant C and is not unique. But, because surface propagators in general satisfy the relations $D^{p\pm}_{yz} = -D^{p\pm}_{zy}$, and after combining with (A2), we find that

$$D^{p\pm}_{yz} = \mp\alpha D^{p\pm}_{yy}. \tag{A11}$$

Because of (A11), the terms in (A10) containing the constant C exactly cancel and we get

$$\begin{aligned} R^p_- &= i\alpha D^{p\,-}_{yy}, \\ R^p_+ &= i\alpha D^{p\,+}_{yy}. \end{aligned} \tag{A12}$$

Expressions (A12) are the generalized reflectivities that now contain both geometric dispersion (i.e., Q dependence) and dispersion due to nonlocal description of electron response included in $D^{p\pm}_{yy}(\mathbf{Q}, i\omega_k)$. Inserting α, one obtains the results given in (42).

*vito@phy.hr
†msunjic@phy.hr
‡lmarusic@unizd.hr

[1] H. B. G. Casimir, Proc. K. Ned. Akad. Wet. **51**, 793 (1948).
[2] R. Esquivel-Sirvent and V. B. Svetovoy, Phys. Rev. B **72**, 045443 (2005).
[3] M. Bostrom and Bo E. Sernelius, Phys. Rev. Lett. **84**, 4757 (2000).
[4] Bo E. Sernelius, J. Phys. A: Math. Gen. **39**, 6741 (2006).
[5] S. K. Lamoreaux, Phys. Rev. Lett. **78**, 5 (1997); **81**, 5475 (1998).
[6] F. Chen, U. Mohideen, G. L. Klimchitskaya, and V. M. Mostepanenko, Phys. Rev. A **72**, 020101(R) (2005).
[7] G. Bressi, G. Carugno, R. Onofrio, and G. Ruoso, Phys. Rev. Lett. **88**, 041804 (2002).
[8] U. Mohideen and Anushree Roy, Phys. Rev. Lett. **81**, 4549 (1998).
[9] Anushree Roy, Chiung-Yuan Lin, and U. Mohideen, Phys. Rev. D **60**, 111101 (1999).

[10]S. K. Lamoreaux, Rep. Prog. Phys. **68**, 201 (2005).
[11]K. A. Milton, J. Phys.: Conf. Ser. **161**, 012001 (2009).
[12]G. L. Klimchitskaya, U. Mohideen, and V. M. Mostepanenko, Rev. Mod. Phys. **81**, 1827 (2009).
[13]A. A. Abrikosov, L. P. Gorkov, and I. E. Dzyaloshinski, *Methods of Quantum Field Theory in Statistical Physics* (Prentice-Hall, Englewood Cliffs, NJ, 1963); see, also, I. E. Dzyaloshinski, E. M. Lifshitz, and L. P. Pitayevski, Usp. Fiz. Nauk **73**, 381 (1961) [Sov. Phys. Usp. **4**, 153 (1961)]; Adv. Phys. **38**, 165 (1961).
[14]E. M. Lifshitz, Zh. Eksp. Teor. Fiz. **29**, 94 (1955) [Sov. Phys. JETP **2**, 73 (1956)].
[15]R. Esquivel, C. Villarreal, and W. L. Mochan, Phys. Rev. A **68**, 052103 (2003).
[16]R. Esquivel and V. B. Svetovoy, Phys. Rev. A **69**, 062102 (2004).
[17]W. L. Mochan, A. M. Contreras-Reyes, R. Esquivel, and C. Villareal, AIP Conf. Proc. **757**, 66 (2005).
[18]R. Esquivel-Sirvent, C. Villarreal, W. L. Mochan, A. M. Contreras-Reyes, and V. B. Svetovoy, J. Phys. A: Math. Gen. **39**, 6323 (2006).
[19]A. M. Contreras-Reyes and W. Luis Mochan, Phys. Rev. A **72**, 034102 (2005).
[20]F. Intravaia and C. Henkel, J. Phys. A: Math. Theor. **41**, 164018 (2008).
[21]Bo E. Sernelius, Phys. Rev. B **71**, 235114 (2005).
[22]Bo E. Sernelius, Phys. Rev. B **74**, 233103 (2006).
[23]Bo E. Sernelius, J. Phys. A: Math. Theor. **41**, 164016 (2008).
[24]V. B. Svetovoy and R. Esquivel, Phys. Rev. E **72**, 036113 (2005); J. Phys. A: Math. Gen. **39**, 6777 (2006).
[25]L. P. Pitaevskii, Phys. Rev. Lett. **101**, 163202 (2008); D. A. R. Dalvit and S. K. Lamoreaux, *ibid*. **101**, 163203 (2008); B. Svetovoy, *ibid.* **101**, 163603 (2008).
[26]P. J. Feibelman, Phys. Rev. B **14**, 762 (1976).
[27]P. J. Feibelman, Phys. Rev. B **23**, 2629 (1981).
[28]Wei Chen and W. L. Schaich, Phys. Rev. B **40**, 5350 (1989).
[29]A. Liebsch, Phys. Rev. B **33**, 7249 (1986).
[30]V. Despoja, M. Šunjić, and L. Marušić, Phys. Rev. B **80**, 075410 (2009).
[31]V. Despoja, M. Šunjić, and L. Marušić, Phys. Rev. B **75**, 045422 (2007).
[32]M. S. Tomaš, Phys. Rev. A **51**, 2545 (1995).
[33]D. M. Newns, Phys. Rev. B **1**, 3304 (1970).
[34]Z. Penzar and M. Šunjić, Phys. Scr. **30**, 431 (1984).
[35]L. Marušić and M. Šunjić, Phys. Scr. **63**, 336 (2001).
[36]V. Despoja, L. Marušić, and M. Šunjić, J. Phys. Condens. Matter **18**, 8217 (2006).
[37]N. W. Ashcroft and N. D. Mermin, *Solid State Physics* (Saunders, Philadelphia, 1976).
[38]J. B. Pendry, J. Phys. Condens. Matter **9**, 10301 (1997); A. I. Volokitin and B. N. J. Persson, J. Phys. Condens. Matter **11**, 345 (1999).